Advanced Materials Research *Online: 2013-12-19*
ISSN: 1662-8985, Vol. 873, pp 174-182
doi:10.4028/www.scientific.net/AMR.873.174

Galvanostatic deposition of Pt nanoparticles on TiO_2 nanotube arrays for amperometric detection of hydrogen peroxide at low overpotentials

Jiaqin Liu[a], Lili Ruan, Guangqing Xu, Jun Lv, Yucheng Wu[b*]

Laboratory of Functional Nanomaterials and Devices, School of Materials Science and Engineering, Hefei University of Technology, Hefei 230009, China

[a]jqliu_hfut@163.com, [b]ycwu@hfut.edu.cn

Keywords: TiO_2 nanotube arrays; Pt nanoparticles; H_2O_2 detection; low overpotential; amperometric method

Abstract: Highly ordered TiO_2 nanotube arrays (NTAs) modified with Pt nanoparticles (Pt/TiO_2 NTAs) have been prepared by anodization of Ti foils followed by electrochemical deposition and employed to improve the performance of the low-overpotential determination of H_2O_2 in solution. Morphologies of TiO_2 and Pt/TiO_2 NTAs were observed by SEM and TEM. The electrochemical behaviors of TiO_2 and Pt/TiO_2 NTAs were compared by cyclic voltammograms (CVs) in phosphate buffer solutions in absence and prensence of 10 mM H_2O_2, which showed that Pt nanoparticles can enhance the electrochemical activities of TiO_2 NTAs and achieve low-overpotential determination of H_2O_2. Amperometric method with an applied potential of -100 mV was used for H_2O_2 detemination, which demonstrated a good H_2O_2 sensing with sensitivity of 5.4 $\mu A \cdot cm^{-2} \cdot mM^{-1}$.

1 Introduction

Design and development of semiconductor nanostructures have drawn significant interest in recent years due to their unique properties and applications[1, 2]. TiO_2 nanostructures, such as TiO_2 nanoparticles fabricated by sol-gel [3], hydrothermal [4] and hydrolysis precipitation techniques [5], and TiO_2 nanotubes by freeze-drying[6], electrodeposition[7], hydrothermal [8], seed growth [9]methods, were extensively studied for their applications of self-cleaning glass [10], photocatalyst [11], dye-sensitized solar cells [12], and photo-electrochemical sensors[13] for organic compound determination because of their photocatalytic performance. TiO_2 nanostructures can absorb the light in the ultraviolet (UV) region and produce electron-hole pairs with excellent redox properties, which can be used for catalytic oxidation of organic compounds and catalytic reduction of metal ions. Wee Y. Gan and coworkers fabricated Pt modified TiO_2 thin films for photocatalytic and photoelectroactalytic degradation of glucose and found that at an applied cathodic potential bias Pt-TiO_2 films displayed higher glucose oxidation efficiency [14].

Since Zwilling and coworkers showed the possibility to grow self-organized and highly ordered TiO_2 nanotube arrays (TiO_2 NTAs) by anodic oxidation of titanium and its alloys [15], great efforts have been employed to improve the morphologies, crystallization and properties of TiO_2 NTAs[16-20]. Daoai Wang and coworkers demonstrated a facile approach to achieve perfectly aligned TiO_2 NTAs with large aspect ratio by two-step anodization [21]. Nageh K. Allam and Craig A. Grimes described a one-step anodization process to fabricate anatase TiO_2 NTAs at room temperature in polyol electrolyte without any further crystallization process [22].

Recently, TiO_2 NTAs have been successfully employed as electrode material in electrochemical sensors [12] and biosensors [23] due to its three-dimensional highly organized structures, semiconductive properties, insertion host capacity, biological compatibility and long-term chemical stability. Based on the photocurrent changes of photocatalytic oxidation of organic compounds, TiO_2 NTAs were achieved for the photoelectrochemical determination of chemical oxygen demand (*COD*) of organic pollutants [12, 24]. Compared with the film-based biosensors, such as PPy film entrapped with glucose oxidase [25], nitrate reductase [26] or phosphorylase [27], biosensors based on TiO_2 NTAs have higher surface area for enzyme

immobilization and enzymatic reaction, which can enhance the detection properties (such as sensitivity, detection limit and linear range) of biosensors. In some oxidase based biosensors, H_2O_2 is the product of enzymatic reaction and the electron transmission medium between enzyme and electrode. Therefore, good electrochemical response to H_2O_2 is the prerequisite for these biosensors to have a good analytic sensitivity.

In this paper, well aligned TiO_2 NTAs were fabricated by anodization of Ti foils in ethylene glycol solution containing 0.3 M NH_4F. Pt nanoparticles were deposited on TiO_2 NTAs to enhance the electrochemical activities and achieve good sensitivity at low overpotential.

2 Experiments

2.1Reagents and Instruments

High purity titanium foil (99.95%) was purchased from Beijing Cuibolin Non-Ferrous Technology Developing Co., Ltd. All other chemicals such as ammonium fluoride (NH_4F), ethylene glycol, potassium chloroplatinate (K_2PtCl_6), sulfuric acid (H_2SO_4), potassium chloride (KCl), hydrogen peroxide (H_2O_2), disodium hydrogen phosphate (Na_2HPO_4), and sodium dihydrogen phosphate (NaH_2PO_4) were analytical reagent grade and purchased from Sigma-Aldrich Company. The supporting electrolyte was 0.05 M phosphate buffer (pH=7) obtained by adjusting the ratio of Na_2HPO_4 to NaH_2PO_4.

TiO_2 NTAs were fabricated using anodization with a voltage-stabilized source (DH 1722A-3). Electrochemical deposition of Pt nanoparticles and H_2O_2 detection were performed using a computerized potentiostat/galvanostat with a three-electrode cell, which was comprised of an Ag/AgCl (3 M KCl saturated) reference electrode, a Pt/Ti wire auxiliary electrode, and working electrode of TiO_2 NTAs fixed on a gold disc. The cyclic voltammetries were performed on an e-corder 410 electrochemical workstation. Morphologies of TiO_2 and Pt/TiO_2 NTAs were observed on scanning electron microscope (JEOL JSM-6300F) and transmission electron microscope (Hitachi H-800).

2.2 Synthetic Procedure

Prior to anodization, titanium foils with diameter of 2 cm were ultrasonically cleaned in acetone and ethanol for 15 min, respectively. The cleaned titanium foils were anodized in ethylene glycol solution containing 0.3 M NH_4F at room temperature for 10 h in a two electrode system. Then the oxidation films were peeled off from the titanium substrate by rinsing with deionized water, and TiO_2 NTAs without barrier layer were thus achieved. TiO_2 NTAs were treated by hydrothermal method at 50℃ for 2 h to achieve crystallization. Then, TiO_2 NTAs were cut into small pieces, and fixed on gold-disc electrode used as working electrode. A 3 M KCl solution saturated Ag/AgCl electrode and a Pt/Ti electrode were used as reference electrode and auxiliary electrode. Electrodeposition of Pt nanoparticles was carried out using the galvanostatic method with a constant cathodic current density of 0.1 mA/cm^2 in a 0.5 M H_2SO_4 solution containing 5 mM K_2PtCl_6. After electrodeposition, the Pt/TiO_2 NTAs electrode was washed with deionized water for several times to remove the residual solution and stored in a phosphate buffer solution at 4℃ in fridge.

2.3 Detection of H_2O_2

Amperometric method used for H_2O_2 detection was carried out in a three-electrode cell with the working electrode of Pt/TiO_2 NTAs array in 2 mL buffer solution (0.05 M, pH 7). The applied potential was determined by the comparison of CVs of NTAs array in buffer solution in absence and presence of H_2O_2. 20 μL H_2O_2 solution with a concentration of 100 mM was injected into 2 mL buffer solution to achieve H_2O_2 increament of around 1 mM. All the curves and relationship between electrochemical response and H_2O_2 concentration were analyzed with the Origin software.

3 Results and discussion

Fig.1 presents the characterizations of TiO_2 and Pt/TiO_2 NTAs. TiO_2 nanotubes fabricated by anodization are non-crystalline, and always annealed at temperatures ranging from 400 to 600℃ to obtain anatase phase. However, the peeled TiO_2 NTAs will roll up when annealing, which is difficult for electrode fixing. Hence, anodized TiO_2 NTAs were hydrothermally treated at 50℃ for 2

h. Fig.1(i) shows the XRD pattern of TiO_2 NTAs. Only anatase phase (2θ = 25.4°, 37.9°, 47.7°, 54°, and 62.5°) can be observed from this pattern, except for the diffraction peaks of titanium metal from the substrate. Peak broadening of anatase phase indicates a nano-scale of anatase crystal grains. The size of these anatase crystal grains calculated by Scherrer equation is around 14 nm.

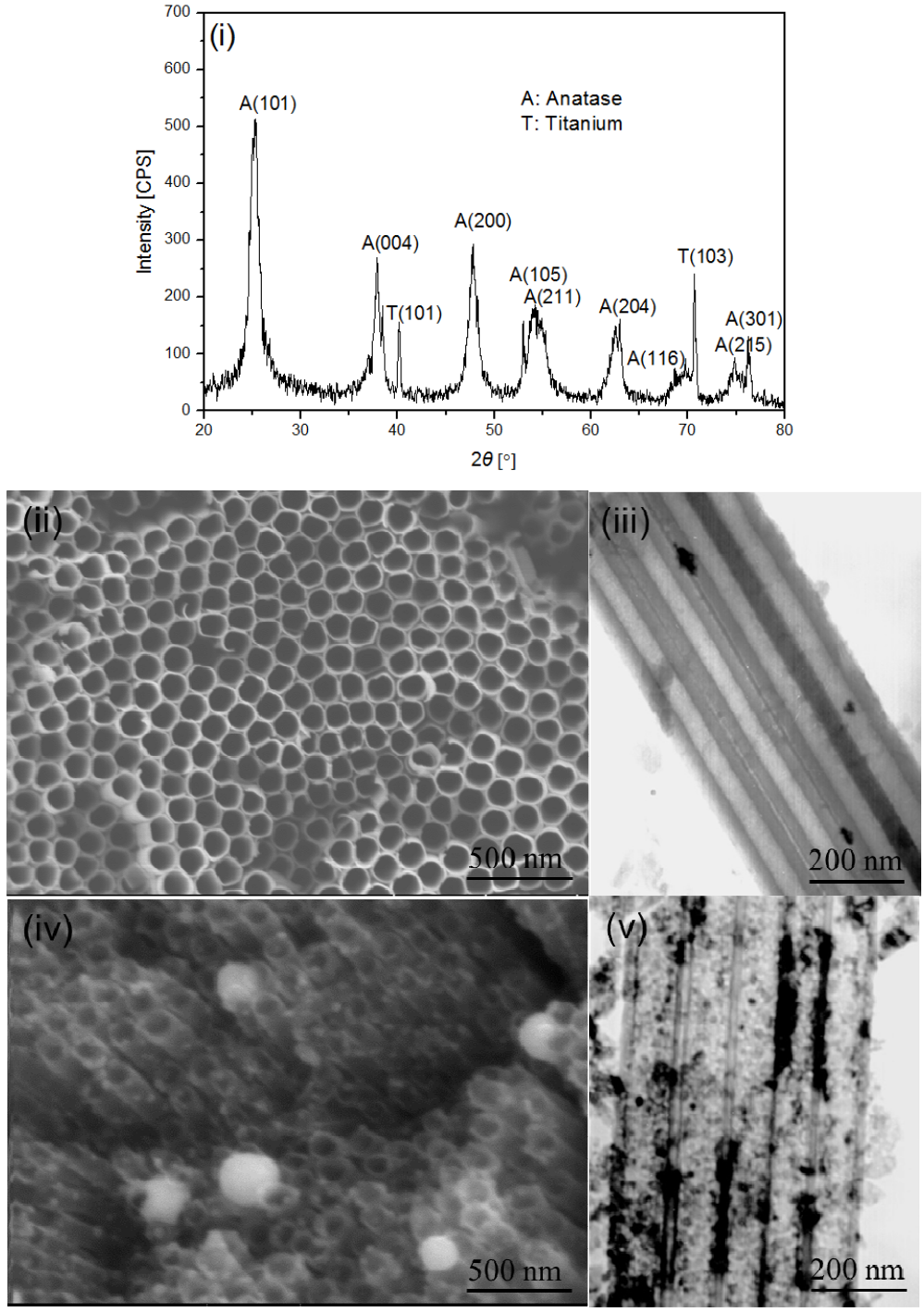

Fig.1 Characterizations of TiO_2 and Pt/TiO_2 NTAs, (i) XRD pattern of TiO_2 NTAs, (ii) SEM morphology of TiO_2 NTAs, (iii) TEM morphology of TiO_2 NTAs, (iv) SEM morphology of Pt/TiO_2 NTAs, and (v) TEM morphology of Pt/TiO_2 NTAs. Fabricating parameters are applied potential of 45 V, anodization time of 10 h, applied Pt deposition current density of -0.1 mA/cm^2 and deposition time of 200 s.

Fig.1(ii) is the top surface morphology of TiO_2 NTAs, showing the vertically aligned and closely packed TiO_2 nanotubes with a diameter of 120 nm on the Ti foil substrate. A single TiO_2 nanotube was observed by TEM and shown in Fig.1(iii). The nanotube was uniform with a diameter of 120 nm and tube wall thickness of 25 nm.

Pt nanoparticles were electrochemically deposited on the walls of TiO_2 nanotubes in a solution containing 0.5 M H_2SO_4 and 5 mM K_2PtCl_6. The SEM mophology of Pt nanoparticle modified TiO_2 NTAs is given in Fig.1(iv). The top view shows that the electrodeposited Pt nanoparticles with a particle size of about 10 nm are in an ordered assembly and uniformly distributed on the tube walls. Some big Pt clusters with diameter of about 200 nm were also observed on the top of NTAs, because on the top surface it is convenient for the ions diffusion to form big particles. Nevertheless, the amount of those clusters is very small. Furthermore, distribution of Pt nanoparticles along the NTAs was examined by TEM and shown in Fig.1(v). It also shows a uniform distribution along the length direction of nanotube.

Fig.2 shows the chronopotentiogram obtained from galvanostatic deposition of Pt nanoparticles on TiO_2 NTAs with current density of -0.1 mA/cm^2. The decrease of potential means the increase of the reduction overpotential in the figure. At the beginning of deposition process, the overpotential increases with time due to the nucleation of Pt on TiO_2 NTAs. The different crystalline structure of Pt from TiO_2 makes a higher overpotential necessary to supply more energy for the nucleation of Pt on TiO_2 surface. The growth of the crystal nucleus requires less energy than that of nucleation, which makes the overpotential decrease sharply after 20 s. The overpotential reaches stable at about 35 s, and then increases with deposition time. The growth rate of Pt crystals is controlled by the diffusion velocity of Pt^{4+} ions in the electric field. The growth rate of Pt crystals is constant with the galvanostatic method. In order to maintain this growth rate, a higher overpotential is necessary to speed the diffusion of Pt^{4+} ions, which results in the increase of overpotetial after 35 s.

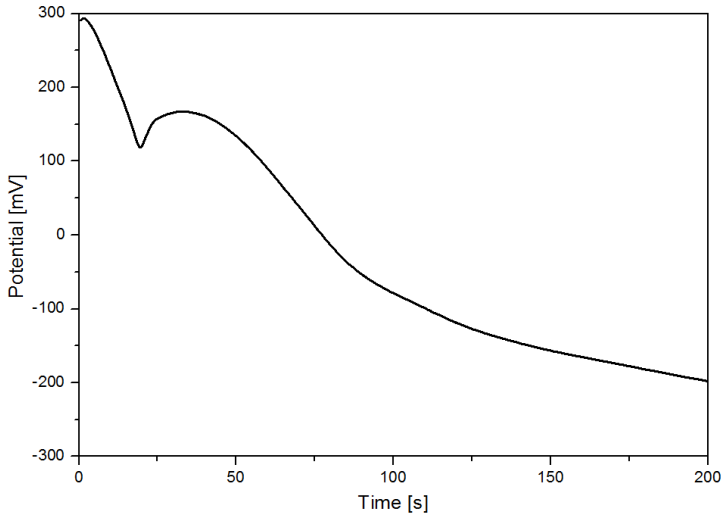

Fig.2 Chronopotentiogram obtained from galvanostatic deposition of Pt nanoparticles on TiO_2 NTAs, solution: 0.5 mM K_2PtCl_6 + 0.5 M H_2SO_4, current density: -0.1 mA/cm^2, deposition time: 200 s.

Fig.3 shows CVs of TiO_2 and Pt/TiO_2 NTAs in a phosphate buffer solution in absence and presence of 10 mM H_2O_2. Fig.3(i) shows the whole comparison of electrochemical behaviors between TiO_2 NTAs in buffer solution in absence (curve (a)) and presence (curve (b)) of 10 mM H_2O_2 and Pt/TiO_2 NTAs in absence (curve (c)) and presence (curve (d)) of 10 mM H_2O_2. To make it more clear, Fig.3(i) is divided into three figures, shown as Fig.3(ii), Fig.3(iii), and Fig.3(iv).

Fig.3(ii) shows the comparison of electrochemical behaviors between TiO_2 and Pt/TiO_2 NTAs in buffer solution. For TiO_2 NTAs, only the current of cathodic hydrogen evolution is detected at potentials lower than -600 mV and the maximum current density is about -200 mA/cm^2. However, the current of cathodic hydrogen evolution (maximum of -800 mA/cm^2 at the potential of -750 mV) and anodic hydrogen desorption (maximum of 650 mA/cm^2 at the potential of -600 mV) of Pt/TiO_2 NTAs are much higher than that of TiO_2 NTAs. The anodic current at positive potentials is due to the anodic oxygen evolution, and the cathodic current peak at the potential of 100 mV is originated from reduction of dissolved O_2 in buffer solution. The higher current response of Pt/TiO_2 NTAs electrode than that of TiO_2 NTAs in the whole potential range indicates that deposited Pt nanoparticles can enhance the electrochemical activity of NTAs.

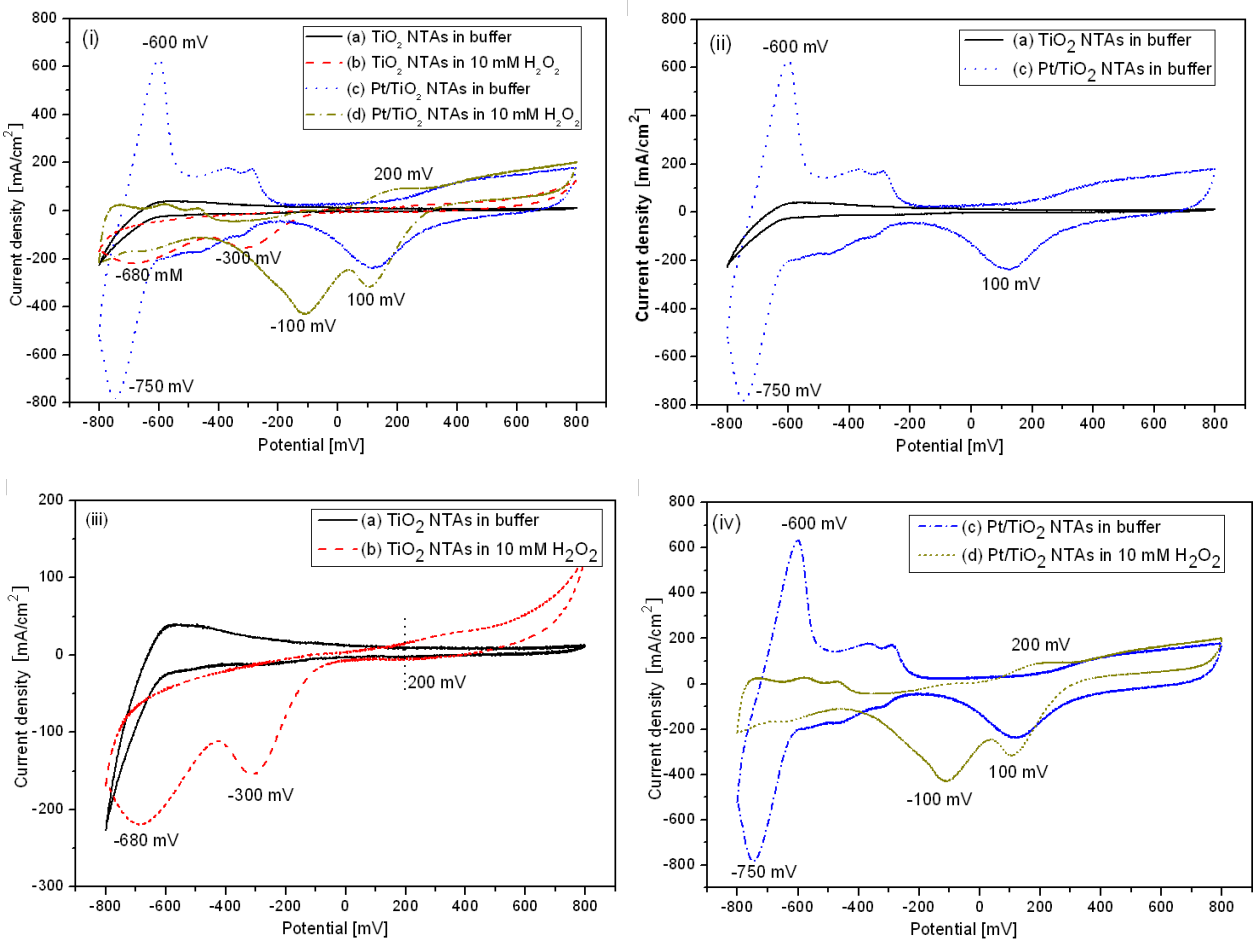

Fig.3 CVs of TiO_2 and Pt/TiO_2 NTAs in phosphate buffer solution in absence and presence of 10 mM H_2O_2 (i); Comparison of CVs between TiO_2 and Pt/TiO_2 NTAs in buffer solution (ii); Comparison of CVs of TiO_2 NTAs in buffer solution in absence and presence of 10 mM H_2O_2 (iii); Comparison of CVs of Pt/TiO_2 NTAs in buffer solution in absence and presence of 10 mM H_2O_2 (iv)

Electrochemical behaviors of TiO_2 NTAs in a buffer solution in absence and presence of 10 mM H_2O_2 are compared in Fig.3(iii). Besides the cathodic hydrogen evolution current at potentials lower than -600 mV, a very small cathodic peak at the potential of -300 mV is observed due to reduction of dissolved oxygen in solution. Evident changes are observed when 10 mM H_2O_2 is added in buffer solution. At potentials higher than 200 mV, anodic current is obtained due to the electrochemical oxidation of H_2O_2 on the surface of TiO_2 NTAs with the following reaction [28]:

$$H_2O_2 \xrightarrow{electrode} O_2 + 2H^+ + 2e^- \quad (1)$$

The oxidation current increases with the increasing applied potential. Two cathodic current peaks can be observed at potentials of -300 mV and -680 mV respectively. The former is same with that of TiO_2 NTAs, which is due to the reduction of dissolved oxygen in solution. However, the current density of this cathodic peak (-160 mA/cm^2) is much higher than that of TiO_2 NTAs in buffer solution because of the O_2 produced in H_2O_2 oxidation process during the positive scanning. Zhang reported that H_2O_2 could be electrochemically reduced at potentials lower than -100 mV[29]. Therefore, the enhancement of this reduction peak is attributed to the combination of reduction of dissolved O_2 produced by H_2O_2 oxidation during the positive scanning and reduction of H_2O_2. The latter is similar to that of TiO_2 NTAs in buffer solution, and it should be originated from the cathodic hydrogen evolution. From reaction (1), H^+ ions are produced from oxidation of H_2O_2, which decreases the overpotential of hydrogen evolution. Therefore, the starting hydrogen evolution potential is about -400 mV, which is higher than that of TiO_2 NTAs in buffer solution (about -600 mV). With the consumption of H^+ ions, the reaction speed of hydrogen evolution was reduced, which causes the decrease of cathodic hydrogen evolution current when the potential is lower than -680 mV.

Comparison of electrochemical behaviors of Pt/TiO_2 NTAs in phosphate buffer solution in absence and presence of 10 mM H_2O_2 is given in Fig.3(iv). Compared with that of Pt/TiO_2 NTAs in buffer solution in absence of H_2O_2, there is a small anodic current peak in presence of 10 mM H_2O_2 at the potential of 200 mV due to the oxidation of H_2O_2. At positive potentials oxygen evolution takes place with the oxidation of both H_2O and H_2O_2. It is easy for H_2O_2 oxidation due to the high electrochemical activity of O^- ions in solution indicated by the lower overpotential for oxygen evolution. The higher current density at the potential of 200 mV of Pt/TiO_2 NTAs in presence of H_2O_2 is due to oxygen evolution from electrochemical oxidation of H_2O_2. At potentials higher than 300 mV, the anodic currents are similar, which can be attributed to the similar reaction velocities of electrochemical oxidation of H_2O and H_2O_2 at high potentials.

The cathodic current peak of Pt/TiO_2 NTAs in H_2O_2 solution originated from the dissolved oxygen reduction at 100 mV is similar to that in buffer solution. The small enhancement of peak current should be related to the oxygen produced from H_2O_2 oxidation during positive scanning. A new cathodic current peak is observed at -100 mV with maximum current density of 450 mA/cm^2 in presence of 10 mM H_2O_2 in the solution, which is higher than that of TiO_2 NTAs (160 mA/cm^2) at applied potential of -300 mV. This new cathodic current peak can be attributed to the reduction of H_2O_2 with the following reaction[28]:

$$H_2O_2 + 2H^+ + 2e^- \xrightarrow{electrode} 2H_2O \quad (2)$$

The presence of H_2O_2 depresses the cathodic hydrogen evolution in the whole negative potential range, which is caused by consumption of H^+ ions in H_2O_2 reduction process according to the reaction (2).

In general, Pt nanoparticles modification can enhance the electrochemical behaviors of TiO_2 NTAs, and achieve higher amperometric responses at relative lower reduction overpotentials.

From the comparison of CVs of TiO_2 and Pt/TiO_2 NTAs in buffer solution in absence and presence of H_2O_2, the applied potentials of amperometric H_2O_2 detection are determined to be -300 mV for TiO_2 NTAs and -100 mV for Pt/TiO_2 NTAs respectively. Fig.4 shows the amperometric detection of H_2O_2 with TiO_2 NTAs and Pt/TiO_2 NTAs respectively. The typical chronoamperograms of TiO_2 NTAs (applied potential of -300 mV) and Pt/TiO_2 NTAs (applied potential of -100 mV) in buffer solution with successive injection of H_2O_2 are shown in Fig.4(i). 20 μL H_2O_2 solution with a concentration of 100 mM was injected into 2 mL buffer solution to give H_2O_2 increment of around 1 mM. The cathodic currents increase stepwise with successive injection of H_2O_2 for both TiO_2 and Pt/TiO_2 NTAs. No amperometric response is observed for TiO_2 NTAs when applied potential is set at -100 mV. And even at potential of -300 mV, the amperometric response is much lower than that of Pt/TiO_2 NTAs. In addition, the shorter response time of Pt/TiO_2 NTAs (ca. 20 s) than that of TiO_2 NTAs (ca. 50 s) to the concentration change of H_2O_2 indicates the better electrochemical behavior of Pt/TiO_2 NTAs.

Calibrations of current density change versus H_2O_2 concentration are shown in Fig.4(ii). The linear relationship between current density change and H_2O_2 concentration of Pt/TiO_2 NTAs is observed clearly in the range from 1 mM to 9 mM fitting the regression equation of I(mA/cm^2) = 0.0012 + 0.0054 C(mM) (correlation coefficient = 0.999). The sensitivity of Pt/TiO_2 NTAs obtained at the potential of -100 mV is 5.4 μA·cm^{-2}·mM^{-1}, which is higher than that of TiO_2 NTAs obtained at the potential of -300 mV (1.56 μA·cm^{-2}·mM^{-1}).

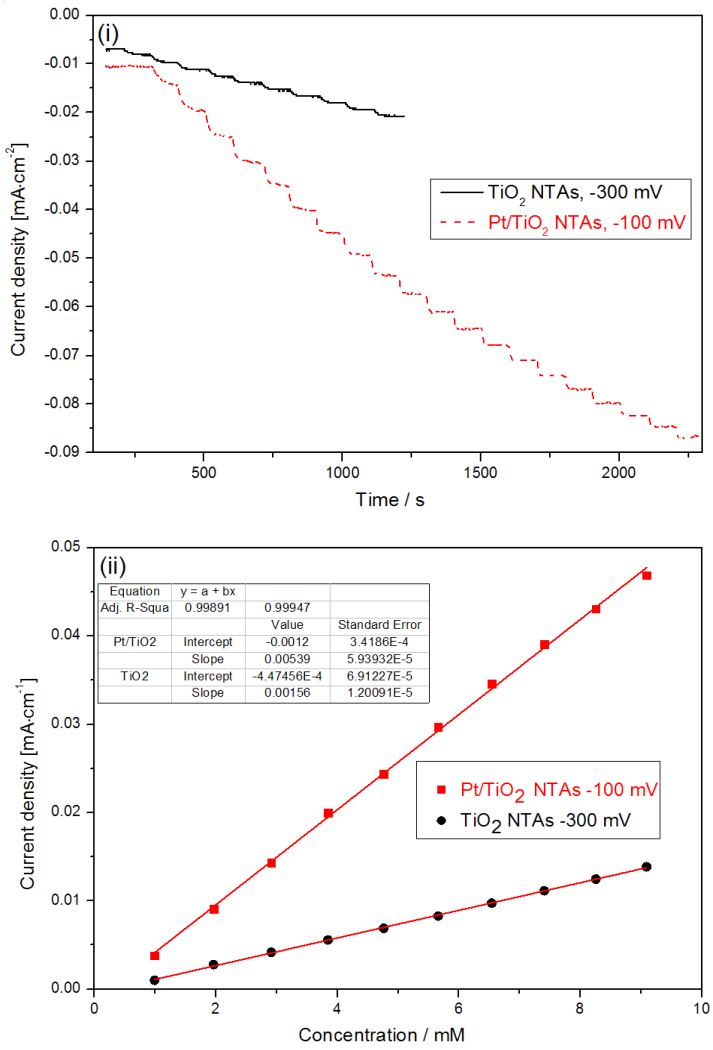

Fig.4 Amperometric detection of H_2O_2 with TiO_2 and Pt/TiO_2 NTAs. (i) Typical chronoamperogram of TiO_2 and Pt/TiO_2 NTAs in buffer solution with successive injection of H_2O_2; (ii) Calibration curves. 20 μL solution containing 100 mM H_2O_2 was injected into 2 mL buffer solution to achieve H_2O_2 increament of around 1 mM.

Pt nanoparticles modification can enhance the electrochemical activities of TiO_2 NTAs and achieve the low potential detection of H_2O_2, which make it possible for many applications of TiO_2 NTAs in the fields of electrochemical sensor and biosensor. Especially in those biosensors with H_2O_2 as the enzymatic reaction product such as glucose biosensor, excellent H_2O_2 sensing can enhance the sensitivity and detection limit of the biosensor. However, electrochemical H_2O_2 sensing of Pt/TiO_2 NTAs is still not as good as that of carbon nanotube modified electrode [30], and horse radish peroxidase (HRP) modified biosensor[31] due to the bad conductivity and the destruction of nanotube structure. Further improvement in the electrochemical properties of TiO_2 NTAs array can be realized by forming mesoporous structures, composite nanoparticles modification and special treatment for crystallization, which can increase the surface area of NTAs array and improve the electronic transmission pathways.

4. Conclusion

Well-alligned TiO_2 NTAs modified with Pt nanoparticles was successfully prepared by anodization combined with galvanostatic deposition. TiO_2 NTAs anodized at voltage of 45 V for 10 h was examined by SEM and TEM to be 120 nm in diameter and 25 nm in tube wall thickness. Pt nanoparticles deposited on TiO_2 NTAs are in an ordered assembly with a uniform distribution and a particle size of 10 nm. Modification of Pt nanoparticles can improve electrochemical activities of TiO_2 NTAs and achieve higher current response of H_2O_2 reduction at the potential of -100 mV. This

overpotential of H_2O_2 reduction on Pt/TiO_2 NTAs (-100 mV) is lower than that on TiO_2 NTAs (-300 mV), which makes it possible for H_2O_2 determination at low overpotentials to avoid interferences. Amperometric method is used for H_2O_2 determination at the applied potential of -100 mV to achieve a sensitivity of 5.4 $\mu A \cdot cm^{-2} \cdot mM^{-1}$ in the range from 1 mM to 18 mM. The possibilities of achieving further improvement in sensitivity and detection limit via forming mesoporous structures, composite nanoparticles modification and special treatment for crystallization are currently being investigated.

Acknowledgements

This work was supported by Nature Science Foundation of China (51102071, 51072044, 51172059), international cooperation project of Anhui Province (10080703017) and the Fundamental Research Funds for the Central Universities (2013HGQC0005).

Reference

[1] X.Y. Zhang, L.H. Xu, J.Y. Dai, Y. Cai, N. Wang. *Mater. Res. Bull.*, 2006, 41(9), 1729-1734.

[2] Y. F. Qiu, M. L. Yang, H. B. Fan, Y. Z.Zuo, Y. Y. Shao, Y. J. Xu, X. X. Yang, S. H. Yang. *Crys. Eng. Comm.*, 2011, 13(6), 1843-1850.

[3] J.H. Richter, P.G. Karlsson, G. Westin, J. Blomquist, P. Uvdal, H. Siegbahn, A. *J. Phys. Chem. C*, 2007, 111(8), 3459-3466.

[4] H.G. Yang, C.H. Sun, S. Z. Qiao, J. Zou, G. Liu, S. C. Smith, H. M. Cheng, G. Q. Lu. *Nature*, 2008, 453(29), 638-641.

[5] J. Fang, F. Wang, K. Qian, H. Z. Bao, Z. Q. Jiang, W. X. Huang. *J. Phys. Chem. C*, 2008, 112(46), 18150-18156.

[6] D. L. Ma, L. S. Schadler, R. W. Siegel, J. I. Hong. *Appl. Phys. Lett.*, 2003, 83, 1839-1841.

[7] Q. Zhang, L. Gao, J. Sun, S. Zheng. *Chem. Lett.* 2002, 2, 226-227.

[8] Daoai Wang, Feng Zhou, Ying Liu, Weimin Liu. *Mater. Lett.*, 2008, 62(12), 1819-1822.

[9] L. Yue, W. Gao, D. Zhang, X. Guo, W. Ding, Y. Chen. *J. Am. Chem. Soc.*, 2006, 128, 11042-11043.

[10] A. Bozzia,T. Yuranovaa, I. Guasaquilloa, D. Laubb, J. Kiwia. *J. Photochem. Photobio. A: Chem.*, 2005, 174(2), 156-164.

[11] J. M. Macak, M. Zlamal, J. Krysa, P. Schmuki. *Small*, 2007, 3(2), 300-304.

[12] Q. Zheng, B. X. Zhou, J. Bai, L. H. Li, Z. J. Jin, J. L. Zhang, J. H. Li, Y. B. Liu, W. M. Cai, X. Y. Zhu. *Adv. Mater.*, 2008, 20(5), 1044-1049.

[13] K. Shankar, G. K. Mor, H. E. Prakasam, O. K. Varghese, C. A. Grimes. *Langmuir*, 2007, 23, 12445-12449.

[14] W. Y. Gan, D. Friedmann, R. Amal, S. Q. Zhang, K. Chiang, H. J. Zhao. *Chem. Eng. J.*, 2010, 158(3), 482-488.

[15] V. Zwilling, M. Aucouturier, E. Darque-Ceretti. *Electrochim. Acta*, 1999, 45(6), 921-929.

[16] S. Yoriya, C. A. Grimes. *Langmuir*, 2010, 26, 417-420.

[17] D. A. Wang, Y. Liu, B. Yu, F. Zhou, W. M. Liu. *Chem. Mater.*, 2009, 21(7), 1198-1206.

[18] M. Paulose, H. E. Prakasam, O. K. Varghese, L. Peng, K. C. Popat, G. K. Mor, T. A. Desai, C. A. Grimes. *J. Phys. Chem. C*, 2007, 111(41), 14992–14997.

[19] C. A. Grimes. J. *Mater. Chem.*, 2007, 17, 1451-1457.

[20] A. Ghicov, P. Schmuki. Chem. Commun. 2009, 2791-2808.

[21] D. A. Wang, B. Yu, C. W. Wang, F. Zhou, W. M. Liu. Adv. Mater., 2009, 21(19), 1962-1967.

[22] N. K. Allam, C. A. Grimes. Langmuir, 2009, 25(13), 7234-7240.

[23] K. S. Mun, S. D. Alvarez, W.Y. Choi, M. J. Sailor. *ACS Nano*, 2010, *4*(4), 2070–2076.

[24] J. Q. Li, L. Zheng, L. P. Li, G. Y. Shi, Y. Z. Xian, L. T. Jin. *Electroanalysis*, 2006, 18(22), 2251-2256.

[25] S. B. Adeloju, A. N. Moline. *Biosens. Bioelectron.*, 2001, 16(3), 133-139.

[26] M. Sohail, S. B. Adeloju. Electroanalysis, 2009, 21(12), 1411-1418

[27] S. B. Adeloju, A. Lawal. Intern. *J. Enviro. Anal. Chem.*, 2005, 85(10), 771-780

[28] Joseph Wang. *Chem. Rev.*, 2008, 108(2), 814–825

[29] X.Y. Zhang, D. Li, L. Bourgeois, H.T. Wang, P.A. Webley. Direct electrodeposition of Porous Gold Nanowire Arrays for Biosensing Applications [J], ChemPhysChem, 2009, 10(2): 436-441

[30] D.R. Shobha Jeykumaria, S. Ramaprabhub, S. Sriman Narayanan. Carbon, 2007, 45(6), 1340-1353.

[31] A.K.M. Kafi,G. S. Wu,A.C. Chen. Biosens. Bioelectron., 2008, 24(4), 566-571.